Nano Energy 79 (2021) 105408

Contents lists available at ScienceDirect

Nano Energy

journal homepage: http://www.elsevier.com/locate/nanoen

A bidirectional direct current triboelectric nanogenerator with the mechanical rectifier

Guangda Qiao [a,b,1], Jianlong Wang [a,b,1], Xin Yu [c,1], Rong Jia [b], Tinghai Cheng [a,b,*], Zhong Lin Wang [a,d,**]

[a] Beijing Institute of Nanoenergy and Nanosystems, Chinese Academy of Sciences, Beijing, 100083, China
[b] School of Mechatronic Engineering, Changchun University of Technology, Changchun, Jilin, 130012, China
[c] School of Electrical and Electronic Engineering, Changchun University of Technology, Changchun, Jilin, 130012, China
[d] School of Materials Science and Engineering, Georgia Institute of Technology, Atlanta, GA, 30332-0245, United States

ARTICLE INFO

Keywords:
Triboelectric nanogenerators
Direct current output
Mechanical rectifier
Energy harvesting

ABSTRACT

The development of direct current triboelectric nanogenerators (DC-TENGs) is of great significance to powering the electronic devices with low consumption. Thus, a bidirectional direct current triboelectric nanogenerator with the mechanical rectifier (BD-TENG) is proposed in this article, which can convert alternating current (AC) generated in the forward and reversed directions into direct current (DC) output without a bridge rectifier. The BD-TENG is comprised of the mechanical structure component, the triboelectric power-generation unit, and the mechanical rectifier. With the operation of the mechanical structure component, AC output generated by the triboelectric power-generation unit is converted into direct current output with the assistance of the mechanical rectifier. The fluorinated ethylene propylene (FEP) films are fabricated into the micro arch structure in the triboelectric power-generation unit, which can harvest the energy in the forward and reversed directions and reduce the friction and wear between materials. And its optimum width is determined through a series of experiments. In addition, the mechanical rectifier is constitutive of the rolling electric brushes and the commutator, which has the advantages of simple structure and low wear. Finally, the BD-TENG can illumine 210 light-emitting diodes (LEDs) and power a commercial calculator directly due to the DC output.

1. Introduction

With the increasing demand for energy in recent years, fossil energy has been affecting the normal operation of the social economy, and even has an influence on the security and stability of some countries. In particular, the rapid development of the electronic devices with low consumption puts forward higher requirements for power-generating devices, such as miniaturized integratebility, functionality and so on [1–5]. However, in terms of micro/small devices, the current mainstream method is to power it through batteries, which generate a series of pollutions and are harmful to the environment. Therefore, developing renewable energy and promoting the utilization of renewable energy have become the inevitable choice to solve the current energy crisis [6–10].

Since 2012, the triboelectric nanogenerators (TENGs) based on the coupling of tribo-electrification and electrostatic induction is invented by professor Wang and his research group for the first time [11–17], which realize the conversion of mechanical energy extensively existing in the environment into electrical energy output. TENGs show a good application prospect in the fields of micro/nano power sources, self-powered sensing, ocean blue energy, and high-voltage power sources and have great scientific research significance in energy sustainable development and environmental protection [18–22]. However, the conventional TENGs have the characteristics of alternating current (AC) output due to the periodic charge transfer between two electrodes. There is no doubt that TENGs connected with a bridge rectifier and power management module at the end of the circuit can meet the actual electricity demand, which not only increases the complexity of the circuit but also results in additional power dissipation. Therefore, the direct current triboelectric nanogenerators (DC-TENGs) are of great

* Corresponding author. Beijing Institute of Nanoenergy and Nanosystems, Chinese Academy of Sciences, Beijing, 100083, China.
** Corresponding author. Beijing Institute of Nanoenergy and Nanosystems, Chinese Academy of Sciences, Beijing, 100083, China.
E-mail addresses: chengtinghai@binn.cas.cn (T. Cheng), zhong.wang@mse.gatech.edu (Z.L. Wang).
[1] These authors contributed equally to this work.

https://doi.org/10.1016/j.nanoen.2020.105408
Received 27 July 2020; Received in revised form 23 August 2020; Accepted 18 September 2020
Available online 23 September 2020

significance to the development of self-powered systems.

So far, there are mainly several approaches to converting AC into direct current (DC). At present, the most common method is to realize DC output by bridge rectifiers, which are extensively applied in self-powered sensing system resulting from the characteristic of stable output. However, the power dissipation brought by bridge rectifiers has an effect on the output performance of TENG. To effectively solve the above problems, electric brushes are applied to the field of TENG [23–25], which has the advantages of simple structure and stable operation. However, the discharge phenomenon and the wear-and-tear are still the main existing problem at present. In addition, some other forms of realizing DC output such as air breakdown [26–30], phase coupling [31–35], schottky diode [36–42] and so forth become mature gradually after several years of unremitting development, which greatly promote the development of DC-TENGs. All in all, the research hotspots of DC-TENGs mainly focus on the reduction of friction and wear between tribo-negative materials and electrode, as well as the power consumption caused by power management module and so on [43–45].

Herein, a bidirectional direct current triboelectric nanogenerator with the mechanical rectifier (BD-TENG) is proposed, which realizes the flow of current and charge in the sole direction. The BD-TENG is constitutive of the mechanical structure component, the triboelectric power-generation unit, and the mechanical rectifier. The mechanical structure part including a rotor and a stator is applied as a support for other components. The triboelectric power-generation unit is comprised of electrodes uniformly distributed in the inner wall of barrel and the fluorinated ethylene propylene (FEP) films fabricated into the micro arch structure, which can not only harvesting the mechanical energy in the forward and reversed directions but also reduce friction and wear between materials. The mechanical rectifier consists of electric brushes and the commutator. Electric brushes are designed to the rolling structure, which can reduce the wear between the electrode brushes and the commutator, and play the role of conduction and commutation of current. The position of commutator corresponds to that of electrodes, which switches the direction of the current. In addition, finite element analysis (FEA) of BD-TENG is performed by using COMSOL Multiphysics 5.5a software and the output performance is measured at different speeds (1 Hz represents 60 rpm). In practical applications, the developed BD-TENG can power a calculator with the assistance of a capacitor and directly illumine 210 light-emitting diodes (LEDs) without a bridge rectifier. Therefore, the BD-TENG will significantly promote the development of DC-TENGs in the self-powered systems.

2. Results and discussion

2.1. Structure design and operating principle

The overall structural design of fabricated BD-TENG is depicted in Fig. 1, which is constitutive of the mechanical structure component, the triboelectric power-generation unit, and the mechanical rectifier (see Fig. 1a). As shown in Fig. 1b, triboelectric power-generation units consist of copper electrodes and the arch fluorinated ethylene propylene (FEP) (see Fig. S1a), which can harvest the energy in the forward and reversed directions, and effectively reduce the friction and wear between materials. The mechanical rectifier is composed of the rolling electric brushes (see Figs. S1b) and a commutator, which can convert the alternating current (AC) generated by the triboelectric power-generation unit into direct current (DC) output, as shown in Fig. 1c.

The photographs of fabricated BD-TENG are shown in Fig. 1d. A barrel and a shaft are embedded in the barrel bracket as a rotor, which rotates under the external excitation through the shaft. And coppers are respectively distributed in the inner wall of the barrel as the electrodes and the outer wall as a commutator as shown in Fig. 1e. Fig. 1f describes that the base with brush holder is regarded as the stator and the arch FEP

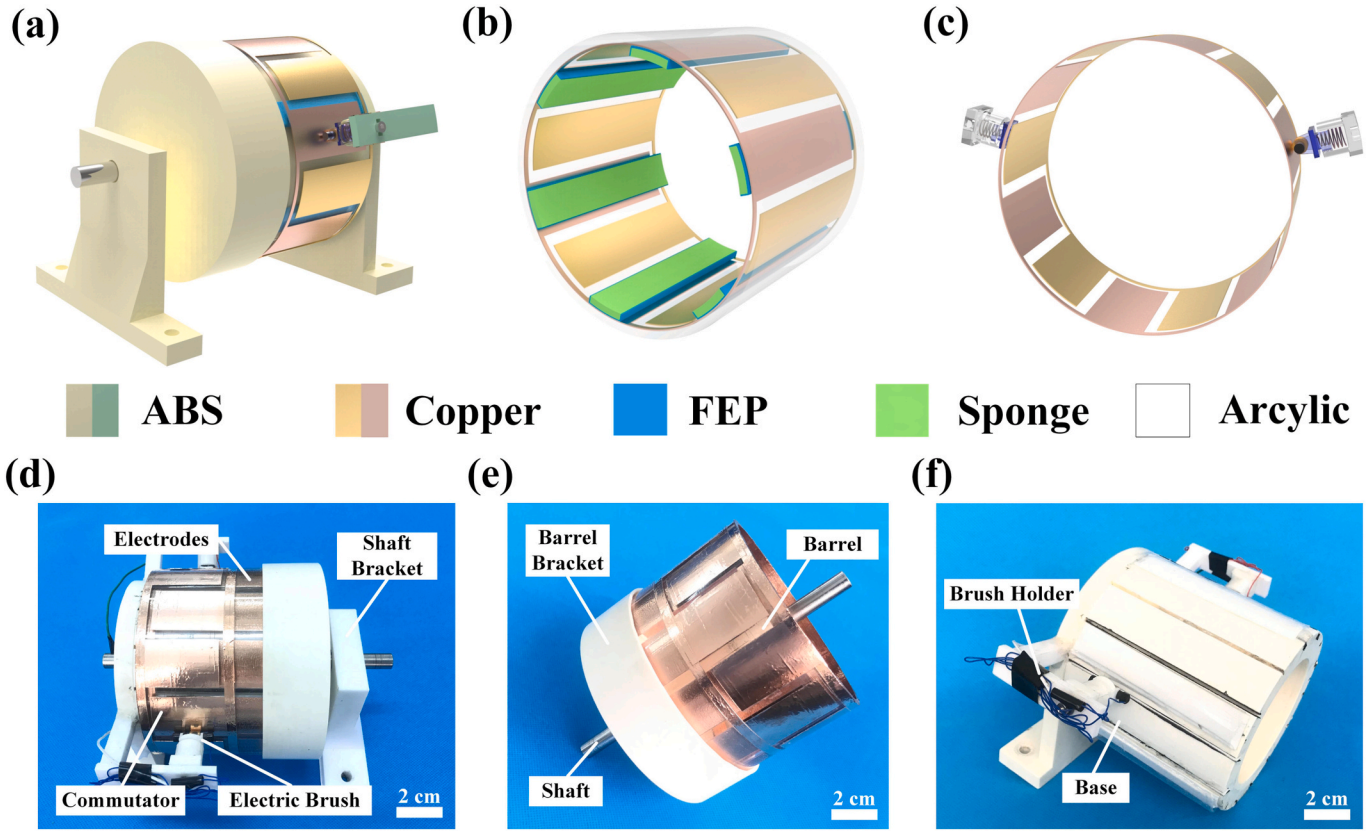

Fig. 1. Structure design drawings of the BD-TENG. (a) Schematic diagram of the overall assembly. (b–c) Partial enlarged photograph of triboelectric power-generation units and the mechanical rectifier. (d–f) Photo of the fabricated BD-TENG, rotor, and stator.

films are uniformly distributed in it. In addition, the mechanical model of electric brush is established and analyzed (see Fig. S2). According to the theoretical calculation, the working frequency adopted in the experiments meets the requirements of theoretical results.

The operating principle of the BD-TENG is shown in Fig. 2a. In the initial state the barrel remains stationary, and the FEP films fixed on the stator are fully contacted with copper-1 which are in the middle position. The electronegativity of copper material is inferior than that of FEP films according to the triboelectric sequence, and it is easier to lose electrons. Based on the principle of tribo-electrification, the surface of copper-1 and FEP films will obtain charge with different properties, respectively [Fig. 2a(i)]. When the barrel with the coppers starts to slide relatively with the FEP films, the copper-1 gradually slides separating from the FEP films and the FEP films begin to gradually contact the copper-2 [Fig. 2a(ii)]. Meanwhile, the electric brush at the left and the right contact copper-2 and copper-1, respectively. The copper-1 will obtain a higher potential due to the transferred charge. Driven by potential difference, the current will flow from copper-2 to copper-1. With the continuous rotation of the barrel with the coppers, the copper-2 will be fully contact with the FEP films [Fig. 2a(iii)]. The contact state and position of the electric brushes and the coppers are in the original state again, and the transferred charge will reach the maximum value at this time. When the barrel with the coppers continues to rotate, the copper-2 gradually separates from the FEP films arranged on the stator. The copper-1 and the FEP films start to slide contact again gradually [Fig. 2a (iv)]. At this time, the electric brush at the left and the right respectively contact copper-1 and copper-2 to complete commutation, realizing DC output. Therefore, it can be seen from the above process that the electric brushes contact with copper-1 and copper-2 alternately, keeping the current direction unchanged.

The COMSOL Multiphysics 5.5a software is employed to clarify the electric potential distributions of BD-TENG to verify the feasibility of the operation principle. Simulation conditions of model are almost consistent with the conventional environment, whose ambient temperature is 293.15 K and the atmosphere pressure is 1 atm. The potential distributions of different positions of coppers and FEP films with a width of 17 mm are analyzed above three situations as shown in Fig. 2b. All materials utilized in the experiment are simulated, whose inherent properties are maintained. The surface charge density of electrodes and FEP films are assumed as the positive charge and the corresponding negative charge, respectively. In addition, the surface charge density is calculated by Equation (S9). Fig. 2b(i) describes the potential distribution of BD-TENG generated by electrostatic induction due to materials contact, the potential difference reaching the maximum value at this time. And then, when the electrodes are gradually sliding separating from the FEP films, the potential difference gradually decreases as shown in Fig. 2b(ii). Fig. 2b(iii) shows that the potential difference gradually increases to the maximum again. Hence, the simulation results prove the feasibility of the BD-TENG in theory.

In order to keep the electric brushes in contact with the commutator during the operation of the rotor and realize the accurate commutation of current, the two electric brushes are installed at a certain angle. The

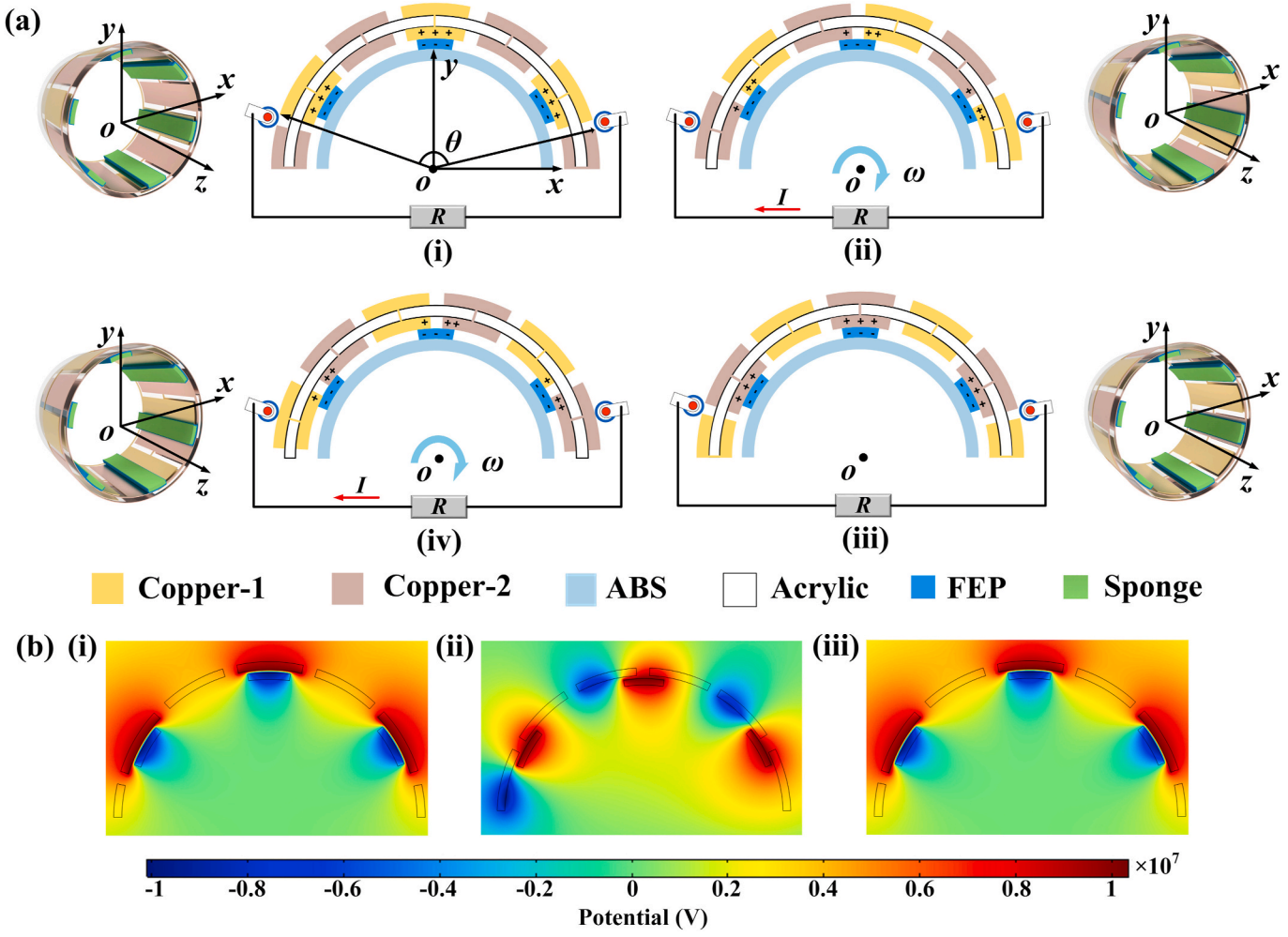

Fig. 2. Schematic diagram showing the operation principle of BD-TENG. (a) Schematic diagram showing the charge distribution and current direction of BD-TENG within a full cycle. (b) The simulation is employed to clarify the electric potential distributions of BD-TENG at three positions by COMSOL software.

installation angle is an odd multiple of the sum of the single copper width and the single copper interval width and thereby, the electric brushes are installed at a fixed angle ($\theta = 150°$) to maintain the symmetry of the electric brushes. Due to the elastic force of the spring, the electric brushes are completely contact with the commutator in the outer wall of barrel which is more conducive to the derivation of current. For the relationship between electric brushes and FEP films, the two electric brushes should respectively contact different coppers to realize DC output at this time when dislocation occurs in the area of arch FEP films and coppers.

2.2. Output performance

The width of FEP films (B_i) and the interval width between the coppers are studied to investigate the feasibility of the whole prototype and verify the influence of different widths of FEP films on output performance. Fig. 3b describes the short-circuit current generated under the action of different widths FEP films and coppers, which can be seen that the discharge phenomenon is generated when the width of FEP films are 25 mm and 20 mm, respectively. A plan view of the relationship among the width of the FEP films, the coppers, and the spacing between the coppers is shown in Fig. 3a. The position of coppers is aligned to the left with the FEP films, and the electric brush-A and the electric brush-B are located at the ends of copper-1 and copper-2, respectively. Taking the left movement as an example, condition 1 is in the initial position when the barrel with the coppers remains stationary. The width of the coppers, the coppers interval width and the width of the FEP films are *l*, *d*, and *l*-*d*, respectively. When the width of FEP films is 25 mm which is consistent with the width of coppers, the discharge phenomenon will occur in the area between the copper-1 and the FEP films. However, the electric brush-A and the electric brush-B do not respectively turn on the copper-2 and copper-1 to complete commutation time resulting in the accumulation of charge, so the discharge phenomenon will appear. When the BD-TENG is in condition 2, it is an intermediate condition with no current flowing. When the coppers keep moving to the left by a distance of *d* and the width of FEP films is 20 mm, the electric brush-A and electric brush-B turn on the copper-2 and copper-1 respectively under the condition 3. And at the next moment, the area will have certain dislocation between coppers and FEP films, the DC output is realized under the action of the electric brushes. Because the flexible material of FEP films will deform, the contact area becomes larger when copper rubs against FEP films. So, it can be seen from Fig. 3b that there will still be the tip discharge when the width of FEP films is 20 mm. When the width of the FEP films exceeds 17 mm, the output performance of the BD-TENG remains almost unchanged and the discharge phenomenon occurs, which will cause damage to the low consumption devices and thereby, FEP films with the width of 17 mm is selected as the experimental optimum parameter.

The measured output performance of the BD-TENG in the forward and reversed directions is shown in Fig. 4. Under the different frequencies, the open-circuit voltage basically remains unchanged, whose open-circuit voltage can reach a maximum of about 480 V as is shown in Fig. 4a. As the working frequency increases, the short-circuit current value also gradually increases, and the short-circuit current value can reach 12 μA at the working frequency of 3 Hz as is depicted in Fig. 4b. Because the charge is in a cumulative condition, Fig. 4c shows linear charging curves in the different speeds, in which it can be seen that with the increase of rotation speed, the time taken to transfer the charge becomes gradually shorten. And when the maximum working frequency is 3 Hz, the time taken to transfer the charge to 15 μC is about 2 s. Fig. 4a–c stipulates that the BD-TENG rotates forward. Similarly, Fig. 4d–f refers to the reversed rotation. From Fig. 4d–f, it can be seen

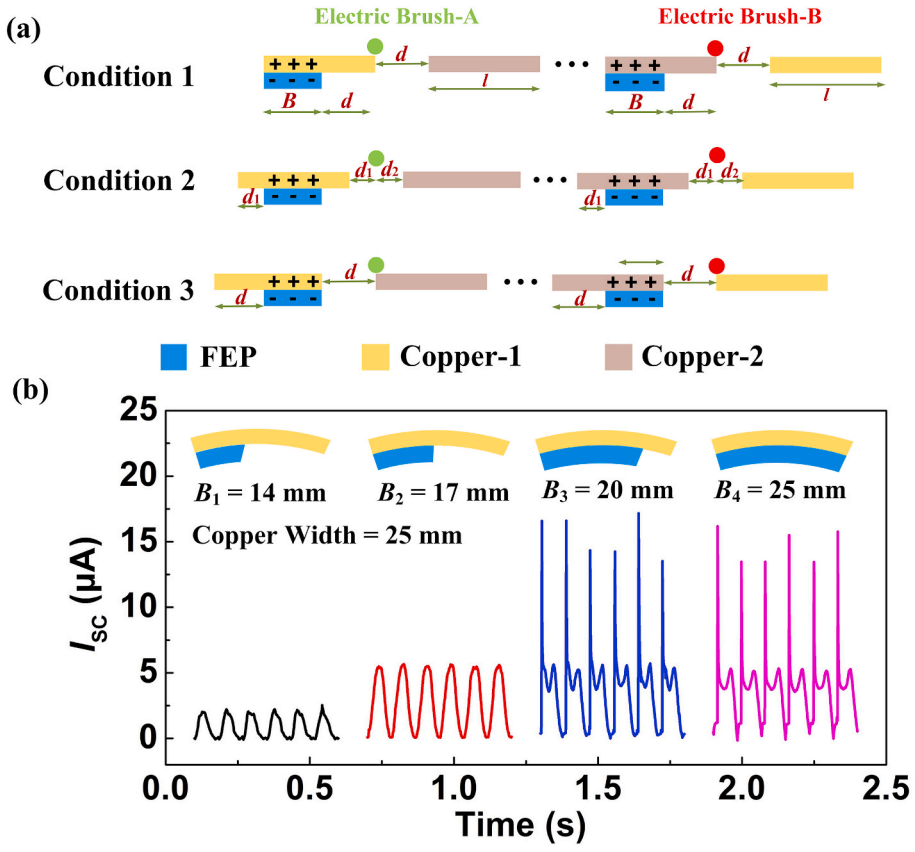

Fig. 3. Relationship diagram between FEP films and electrodes of BD-TENG. (a) The derived diagram of operation principle between FEP films and electrodes. (b) Schematic showing the output performance of BD-TENG with FEP films of different widths (B_i) and electrodes of identical widths at the working frequency of 1 Hz.

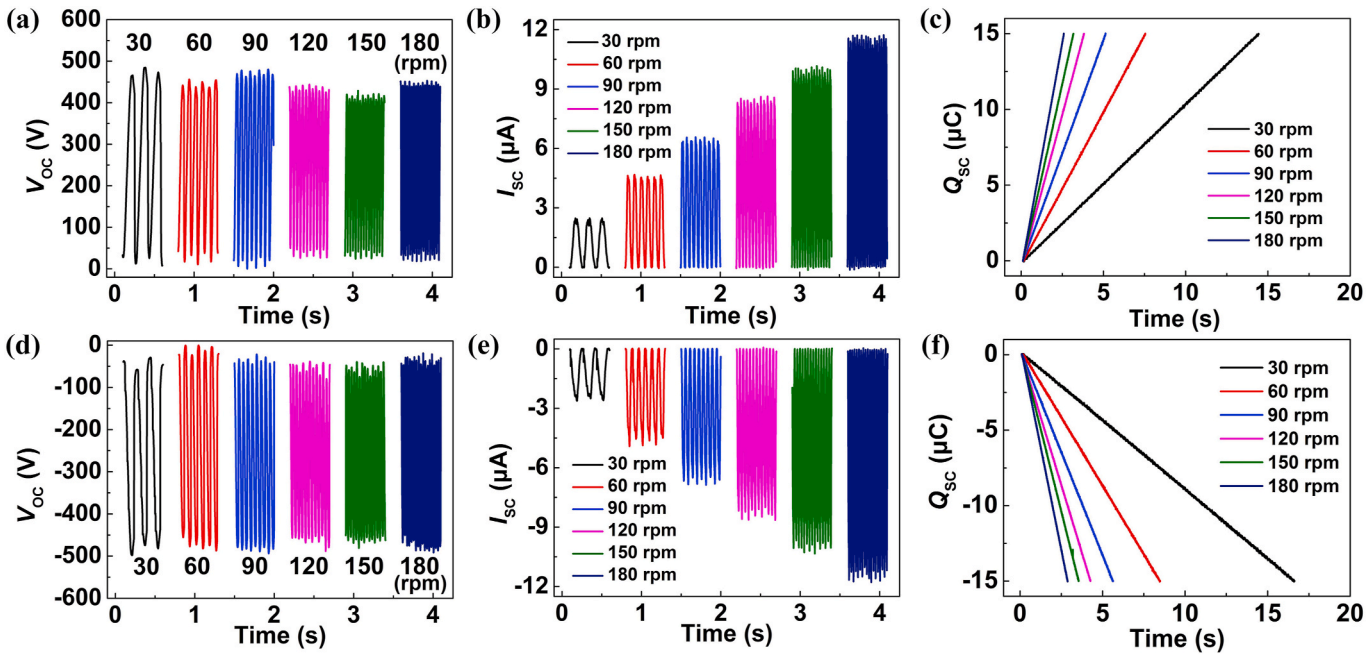

Fig. 4. The output performance of BD-TENG at different rotation speeds in the forward direction (a–c) and in the reversed rotation (d–f), respectively.

that the output performance of reversed direction is basically in accordance with that of forward direction.

2.3. Demonstration

In order to better describe the application capability of the BD-TENG, the current generated by the BD-TENG is DC under the action of electric brushes without a bridge rectifier. Fig. 5a depicts a physical diagram and an equivalent circuit diagram of a 1.0 μF capacitor charged by the BD-TENG, which can be seen that a 1.0 μF capacitor can be directly charged without a bridge rectifier. Fig. 5b shows the curve of charging a 1.0 μF capacitor at different frequencies. As the working frequency increases, the shorter the time it takes, the higher the efficiency it is. When the working frequency of external excitation is 3 Hz, the commercial capacitor can be charged to 10 V in about 2 s. Fig. 5c is the relation curve between short-circuit current and power of BD-TENG under different load resistances. The output power can be calculated by the load current and the load impedance of the external circuit. According to the experimental data, a conclusion can be reached that when the external load impedance is 100 MΩ, the maximum output power of 0.96 W/m^2 can be obtained at the working frequency of 3 Hz.

In addition, the platform based on the BD-TENG is established to prove that the BD-TENG can harvesting mechanical energy in both directions, and lighting experiments are conducted in the forward and

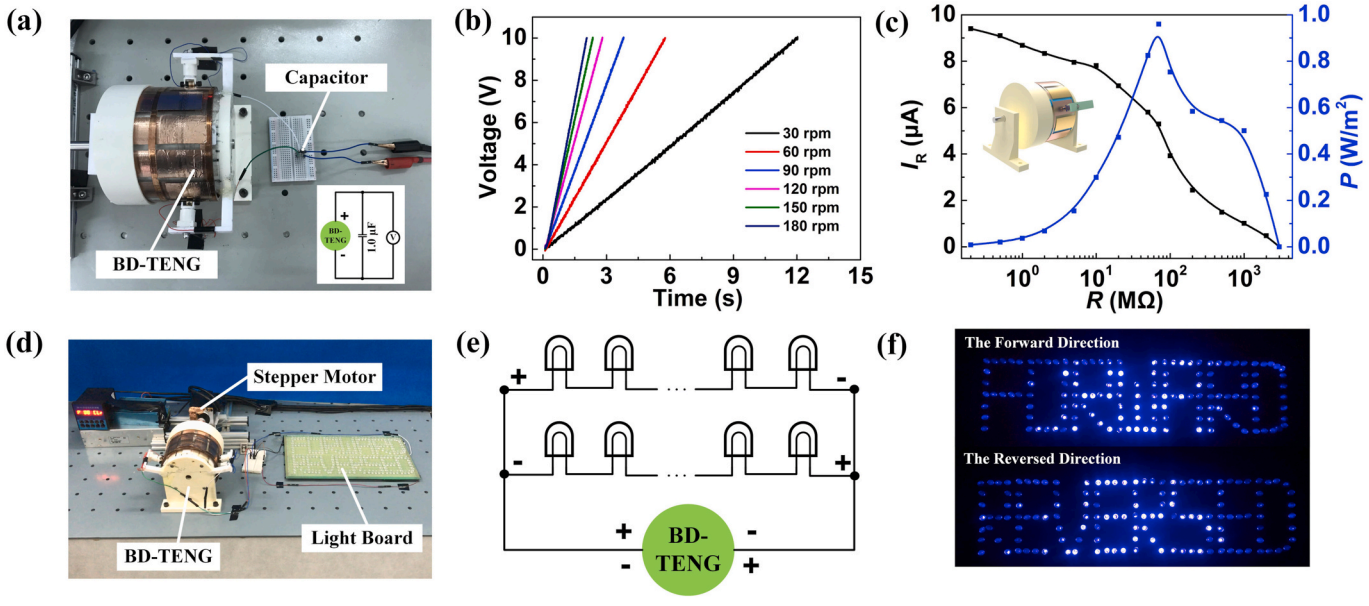

Fig. 5. Electrical measurements of BD-TENG under the excitation of the motor. (a) Photo showing the BD-TENG charges a 1.0 μF capacitor without a bridge rectifier. (b) The charging time required is measured for a 1.0 μF capacitor from 0 V to 10 V at different speeds. (c) Relationship curve between load current and output power at the working frequency of 3 Hz. (d) Photograph of the platform based on the BD-TENG for harvesting mechanical energy in both directions. (e) Equivalent circuit diagram of the "FORWARD" and "REVERSED" LEDs. (f) Photograph of the "FORWARD" and "REVERSED" LEDs driven by the BD-TENG.

reversed directions as is depicted in Fig. 5d. Fig. 5e shows the equivalent circuit under this experiment, which is connected in parallel after two rows of LEDs are connected in series. And the positive and negative poles of the LEDs in the upper row are opposite to those in the lower row. From Fig. 5f and Movie S1, "FORWARD" and "REVERSED" LEDs can be lit steadily without a bridge rectifier in the forward and reversed directions, respectively.

Supplementary data related to this article can be found at https://doi.org/10.1016/j.nanoen.2020.105408.

In order to prove that the BD-TENG can be employed as a reliable power supply in practical applications, the BD-TENG is applied to illumine light-emitting diodes (LEDs) in series and power a commercial calculator under the simulated wind environment of approximately 7 m/s by a blower. Fig. 6a and b shows the experimental measurement platform and equivalent circuit diagram of BD-TENG harvesting wind energy to power LEDs. A blower is used to simulate the real wind environment and drive the wind scoop to rotate. Fig. 6c and Movie S2 show that BD-TENG can light 210 LEDs in series under the wind blowing condition without a bridge rectifier. As is depicted in Fig. 6, the experimental platform based on the BD-TENG is established to harvest the wind energy, which realize the stable DC output to power a commercial calculator with the assistance of a 100 μF capacitor. The experimental results show that the calculator can be powered stably (see Fig. 6e), and the voltage curves of the capacitor are plotted in Fig. 6f. The BD-TENG can directly charge the voltage of capacitor to 1.5 V in 28 s without a bridge rectifier and then, the calculator starts to work steadily (Movie S3).

Supplementary data related to this article can be found at https://doi.org/10.1016/j.nanoen.2020.105408.

3. Conclusions

In summary, the prototype BD-TENG is proposed to realize the convertion of mechanical energy in the environment into direct current (DC) output without a bridge rectifier. Thus, the problem of power dissipation caused by the power management module which is complicated and complex can be effectively solved, and the high output performance is obtained. The flexible fluorinated ethylene propylene (FEP) films are fabricated into the micro arch structure, which can reduce friction and wear between materials and harvest energy in the forward and reversed directions, whose output performance is almost identical in both conditions. In addition, arch FEP films with the optimum width are selected through the experiments. And rolling electric brushes are applied to the field of triboelectric nanogenerators (TENGs) to convert alternating current (AC) into DC output, which reduced the wear between electrode brushes and the commutator. A series of experiments have been conducted and the experimental results show that the BD-TENG can produce the open-circuit voltage of 480 V and short-circuit current 12 μA and the time taken to transfer the charge to 15 μC is about 2 s at the working frequency of 3 Hz. And the power density of about 0.96 W/m^2 is obtained at an identical working frequency. In addition, the BD-TENG can charge a 1.0 μF commercial capacitor to 10 V in 2 s and illumine 210 light-emitting diodes (LEDs) without a bridge rectifier. In practical applications, it can also power a calculator steadily at a wind speed of approximately 7 m/s. It is believed that the BD-TENG will have a good application prospect in the fields of micro/nano power sources.

4. Experimental section

4.1. Fabrication of the BD-TENG

The BD-TENG is comprised of a stainless steel shaft, a shaft bracket, electrodes, flexible thin films, a commutator, bearings (SC6700zz, NSK, Japan), a barrel, a barrel bracket, two electric brushes, two brush holders and a base. A barrel with dimensions of 105 mm (external diameter) × 99 mm (inner diameter) × 110 mm (length) and bearings are obtained by commercial means. Electrodes distributed in the inner wall of barrel is fabricated by the copper whose sizes are 90 mm (length) × 99 mm (diameter). In addition, the copper with a length of 40 mm in the external diameter is applied to the commutator. The different width of flexible thin films distributed in the outer wall of stator are made of fluorinated ethylene propylene (FEP) whose sizes are 90 mm (length) × 100 μm (thickness). A shaft bracket, a barrel bracket, two brush holders and a base are fabricated by a 3D printer with polylactic acid (PLA) material, and the stainless steel shaft is machined by the lathes.

4.2. Electrical measurement

A two-phase hybrid stepper motor (J-5718HBS401, Longshun,

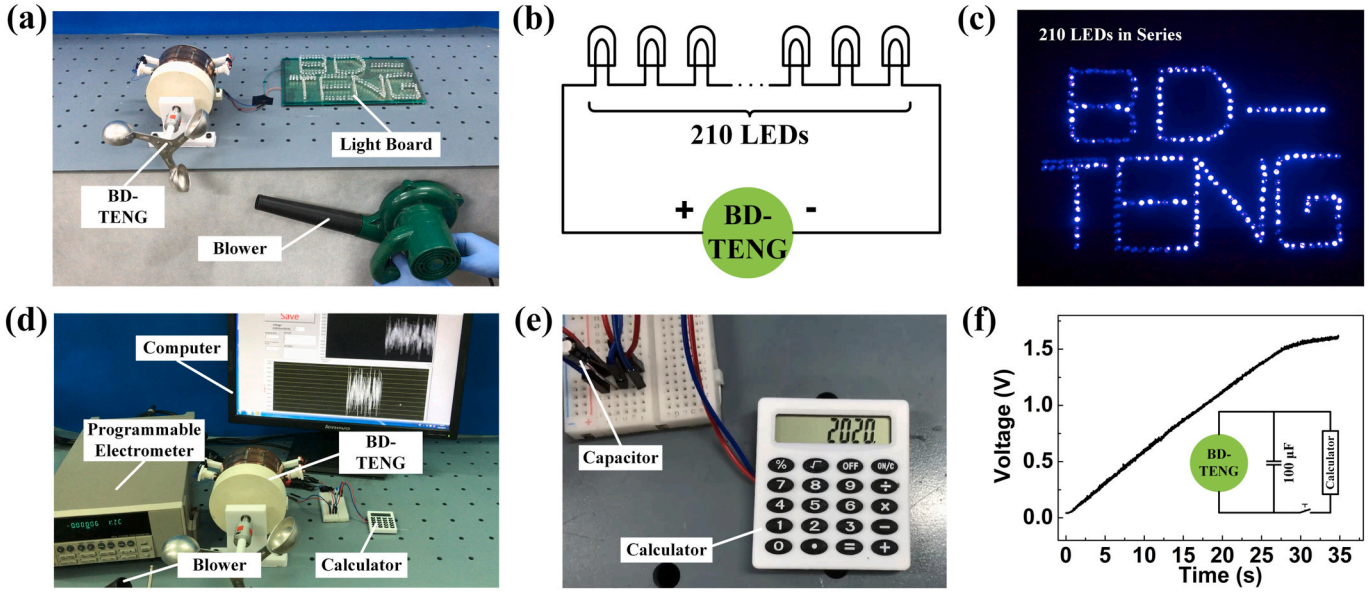

Fig. 6. Demonstration of BD-TENG as a practical power source under the simulated wind environment. (a–b) Experimental measurement platform and equivalent circuit diagram of BD-TENG harvesting wind energy to power LEDs. (c) The BD-TENG can directly light up 210 LEDs in series. (d–e) Schematic diagram showing the experimental system and enlargement display of calculator energy supply. (f) Energy supply curve of BD-TENG.

China) is applied as the experimental power output equipment, which is connected to the BD-TENG with the assistance of a rigid coupling. Then, a programmable electrometer (6514, Keithley, USA) and a data acquisition system (PCI-6259, National Instruments, USA) are utilized for collecting the output signal of BD-TENG, which is processed and stored by a programmed LabVIEW software and a computer (ThinkCentre M8500t-N000, Lenovo, China), respectively. The scanning electron microscope images are taken by scanning electron microscopy (SU8020, HITACHI, Japan).

CRediT authorship contribution statement

Guangda Qiao: Conceptualization, Investigation. **Jianlong Wang:** Conceptualization, Writing - original draft, Writing - review & editing. **Xin Yu:** Writing - original draft, Writing - review & editing. **Rong Jia:** Investigation. **Tinghai Cheng:** Conceptualization, Resources, Investigation, Writing - original draft, Writing - review & editing, Supervision. **Zhong Lin Wang:** Conceptualization, Resources, Investigation, Writing - original draft, Writing - review & editing, Supervision.

Declaration of competing interest

The authors declare that they have no known competing financial interests or personal relationships that could have appeared to influence the work reported in this paper.

Acknowledgments

Guangda Qiao, Jianlong Wang and Xin Yu contributed equally to this work. The authors are grateful for the support received from the National Key R&D Project from the Minister of Science and Technology (2016YFA0202704), the Beijing Municipal Science and Technology Commission (Z171100002017017), and the National Natural Science Foundation of China (51775130).

Appendix A. Supplementary data

Supplementary data to this article can be found online at https://doi.org/10.1016/j.nanoen.2020.105408.

References

[1] Q. Schiermeier, J. Tollefson, T. Scully, A. Witze, O. Morton, Nature 454 (2008) 816–823.
[2] Z.L. Wang, Nature 542 (7640) (2017) 159–160.
[3] Z. Wu, T. Cheng, Z.L. Wang, Sensors 20 (10) (2020) 2925.
[4] W. Xu, H. Zheng, Y. Liu, X. Zhou, C. Zhang, Y. Song, X. Deng, M. Leung, Z. Yang, R. X. Xu, Z.L. Wang, X.C. Zeng, Z. Wang, Nature 578 (7795) (2020) 392–396.
[5] K. Xia, D. Wu, J.M. Fu, Z. Xu, Nano Energy 77 (2020) 105112.
[6] M. Bouza, Y. Li, C. Wu, H. Guo, Z.L. Wang, F.M. Fernandez, J. Am. Soc. Mass Spectrom. 31 (3) (2020) 727–734.
[7] X. Chen, L. Gao, J. Chen, S. Lu, H. Zhou, T. Wang, A. Wang, Z. Zhang, S. Guo, X. Mu, Z.L. Wang, Y. Yang, Nano Energy 69 (2020) 104440.
[8] S.-F. Leung, H.-C. Fu, M. Zhang, A.H. Hassan, T. Jiang, K.N. Salama, Z.L. Wang, J.-H. He, Energy Environ. Sci. 13 (5) (2020) 1300–1308.
[9] H. Zou, G. Dai, A.C. Wang, X. Li, S.L. Zhang, W. Ding, L. Zhang, Y. Zhang, Z. L. Wang, Adv. Mater. 32 (11) (2020) 1907249.
[10] J. Qian, J. He, S. Qian, J. Zhang, X. Niu, X. Fan, C. Wang, X. Hou, J. Mu, W. Geng, X. Chou, Adv. Funct. Mater. 30 (4) (2019) 1907414.
[11] F.-R. Fan, Z.-Q. Tian, Z.L. Wang, Nano Energy 1 (2) (2012) 328–334.
[12] S. Lin, L. Xu, A.C. Wang, Z.L. Wang, Nat. Commun. 11 (1) (2020) 399.
[13] K. Xia, Z. Zhu, H. Zhang, C. Du, Z. Xu, R. Wang, Nano Energy 50 (2018) 571–580.
[14] Z.L. Wang, Faraday Discuss 176 (2014) 447–458.
[15] Z.L. Wang, Nano Energy 54 (2018) 477–483.
[16] Z.L. Wang, Nano Energy 68 (2020) 104272.
[17] J. Yu, X. Hou, M. Cui, S. Zhang, J. He, W. Geng, J. Mu, X. Chou, Nano Energy 64 (2019) 103923.
[18] J. Nie, Z. Ren, L. Xu, S. Lin, F. Zhan, X. Chen, Z.L. Wang, Adv. Mater. 32 (2) (2019) 1905696.
[19] Z.L. Wang, Mater. Today 20 (2) (2017) 74–82.
[20] Z.L. Wang, Adv. Energy Mater. 10 (17) (2020) 2000137.
[21] Z.L. Wang, A.C. Wang, Mater. Today 30 (2019) 34–51.
[22] K. Xia, J. Fu, Z. Xu, Adv. Energy Mater. 10 (28) (2020) 2000426.
[23] D. Liu, J.-F. Bao, Y.-L. Chen, G.-K. Li, X.-S. Zhang, Nano Energy 74 (2020) 104770.
[24] J. Wang, Z. Wu, L. Pan, R. Gao, B. Zhang, L. Yang, H. Guo, R. Liao, Z.L. Wang, ACS Nano 13 (2) (2019) 2587–2598.
[25] C. Zhang, T. Zhou, W. Tang, C. Han, L. Zhang, Z.L. Wang, Adv. Energy Mater. 4 (9) (2014) 1301798.
[26] D. Liu, X. Yin, H. Guo, L. Zhou, X. Li, C. Zhang, J. Wang, Z.L. Wang, Sci. Adv. 5 (4) (2019), eaav6437.
[27] C. Chen, H. Guo, L. Chen, Y.C. Wang, X. Pu, W. Yu, F. Wang, Z. Du, Z.L. Wang, ACS Nano 14 (4) (2020) 4585–4594.
[28] J. Luo, L. Xu, W. Tang, T. Jiang, F.R. Fan, Y. Pang, L. Chen, Y. Zhang, Z.L. Wang, Adv. Energy Mater. 8 (27) (2018) 1800889.
[29] G. Xu, D. Guan, X. Yin, J. Fu, J. Wang, Y. Zi, EcoMat 2 (3) (2020), e12037.
[30] Y. Yang, H. Zhang, Z.L. Wang, Adv. Funct. Mater. 24 (24) (2014) 3745–3750.
[31] X. Li, X. Yin, Z. Zhao, L. Zhou, D. Liu, C. Zhang, C. Zhang, W. Zhang, S. Li, J. Wang, Z.L. Wang, Adv. Energy Mater. 10 (7) (2020) 1903024.
[32] T. Kim, D.Y. Kim, J. Yun, B. Kim, S.H. Lee, D. Kim, S. Lee, Nano Energy 52 (2018) 95–104.
[33] H. Ryu, J.H. Lee, U. Khan, S.S. Kwak, R. Hinchet, S.-W. Kim, Energy Environ. Sci. 11 (8) (2018) 2057–2063.
[34] J. Wang, Y. Li, Z. Xie, Y. Xu, J. Zhou, T. Cheng, H. Zhao, Z.L. Wang, Adv. Energy Mater. 10 (10) (2020) 1903024.
[35] M.-H. Yeh, H. Guo, L. Lin, Z. Wen, Z. Li, C. Hu, Z.L. Wang, Adv. Funct. Mater. 26 (7) (2016) 1054–1062.
[36] S. Lin, Y. Lu, S. Feng, Z. Hao, Y. Yan, Adv. Mater. 31 (7) (2019) 1804398.
[37] J. Liu, A. Goswami, K. Jiang, F. Khan, S. Kim, R. McGee, Z. Li, Z. Hu, J. Lee, T. Thundat, Nat. Nanotechnol. 13 (2) (2018) 112–116.
[38] H. Shao, J. Fang, H. Wang, L. Dai, T. Lin, Adv. Mater. 28 (7) (2016) 1461–1466.
[39] H. Shao, J. Fang, H. Wang, H. Niu, H. Zhou, Y. Cao, F. Chen, S. Fu, T. Lin, Nano Energy 62 (2019) 171–180.
[40] H. Shao, J. Fang, H. Wang, H. Zhou, T. Lin, J. Mater. Chem. A 5 (18) (2017) 8267–8273.
[41] H. Shao, J. Fang, H. Wang, H. Zhou, H. Niu, F. Chen, G. Yan, S. Fu, Y. Cao, T. Lin, Adv. Electron. Mater. 5 (2) (2018) 1800675.
[42] Z. Zhang, D. Jiang, J. Zhao, G. Liu, T. Bu, C. Zhang, Z.L. Wang, Adv. Energy Mater. 10 (9) (2020) 1903713.
[43] S. Park, H. Ryu, S. Park, H. Hong, H.Y. Jung, J.-J. Park, Nano Energy 33 (2017) 184–194.
[44] P. Wang, L. Pan, J. Wang, M. Xu, G. Dai, H. Zou, K. Dong, Z.L. Wang, ACS Nano 12 (9) (2018) 9433–9440.
[45] Y. Zhong, H. Zhao, Y. Guo, P. Rui, S. Shi, W. Zhang, Y. Liao, P. Wang, Z.L. Wang, Adv. Mater. Tech. 4 (12) (2019) 1900741.

Guangda Qiao received the B.E. degree from the School of Mechatronics Engineering at the Changchun University of Technology in 2019. He is currently working toward the M.S. degree in mechanical Engineering at the same school. His work is focused on triboelectric nanogenerators and piezoelectric actuators.

Jianlong Wang majored in mechanical engineering and received his B.E. degree from Changchun University of Technology. He is currently a master degree candidate under the supervision of Prof. Tinghai Cheng in the same school. His research interest is in the area of triboelectric nanogenerators.

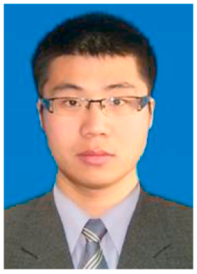

Dr. Xin Yu is a lecturer in the College of Electrical and Electronic Engineering, Changchun University of Technology. He obtained the B.S. and Ph.D. degrees from College of Electronic Science and Engineering, Jilin University in 2009 and 2014. He was a visiting scholar in the WAVES Lab, Department of Electrical and Computer Engineering, Michigan State University from 2017 to 2018. His interests are triboelectric nanogenerators, infrared gas sensing and photoelectric information detection.

Rong Jia was born in Shanxi, China. He graduated Changchun University of Technology in 2020, and acquired B.S. degree in the school of mechatronic engineering. He continues his studies at the Xi'an Jiaotong University. He has research interests in the area of triboelectric nanogenerators and their applications.

Prof. Tinghai Cheng received the B.S., M.S. and Ph.D. degrees from Harbin Institute of Technology in 2006, 2008 and 2013, respectively. He was a visiting scholar in the School of Materials Science and Engineering at Georgia Institute of Technology under the supervision of Prof. Zhong Lin (Z. L.) Wang from 2017 to 2018. He now works as a professor in Beijing Institute of Nanoenergy and Nanosystems, Chinese Academy of Sciences (CAS). His research interests are triboelectric nanogenerators, piezoelectric energy harvester, and piezoelectric actuators.

Prof. Zhong Lin Wang received his Ph.D. from Arizona State University in physics. He now is the Hightower Chair in Materials Science and Engineering, Regents' Professor, Engineering Distinguished Professor and Director, Center for Nanostructure Characterization, at Georgia Tech. Dr. Wang has made original and innovative contributions to the synthesis, discovery, characterization and understanding of fundamental physical properties of oxide nanobelts and nanowires, as well as applications of nanowires in energy sciences, electronics, optoelectronics and biological science. His discovery and breakthroughs in developing nanogenerators established the principle and technological road map for harvesting mechanical energy from environment and biological systems for powering personal electronics. His research on self-powered nanosystems has inspired the worldwide effort in academia and industry for studying energy for micro-nano-systems, which is now a distinct disciplinary in energy research and future sensor networks. He coined and pioneered the field of piezotronics and piezophototronics by introducing piezoelectric potential gated charge transport process in fabricating new electronic and optoelectronic devices. Details can be found at: http://www.nanoscience.gatech.edu.